Agile adaptive radar sampling of fast-evolving atmospheric phenomena guided by satellite imagery and surface cameras

Pavlos Kollias[1,2], Edward Luke[2], Mariko Oue[1] and Katia Lamer[2]

1. Division of Atmospheric Sciences, Stony Brook University, Stony Brook, NY USA
2. Environmental and Climate Sciences Dept., Brookhaven National Laboratory, Upton NY USA

Corresponding author:

Pavlos Kollias
Division of Atmospheric Sciences
School of Marine and Atmospheric Sciences
Stony Brook University
Email: pavlos.kollias@stonybroook.edu

Abstract

The collection of high temporal resolution radar observations without compromising data quality requires adaptability and agility. So far, radar beam steering has been mostly guided by i) the expert judgment or ii) stand-alone automated identification and tracking algorithms operating on measurements collected by the radar itself. The current study proposes a new paradigm, where external observations are used to optimize a radar's sampling strategy. Here the sampling strategy of a phased-array radar and a polarimetric scanning cloud radar, two different yet uniquely complementary systems, is guided by an algorithm that uses observations from a geostationary satellite, a surface camera and the radars themselves to identify and track atmospheric phenomena. The tailored pointing and increase in sensitivity realized through this framework enables the steered radars to sample a diverse set of atmospheric phenomena such as shallow cumuli, lightning-induced ice crystal orientation and a series of waterspouts.

1. Introduction

Since the early 1960's, radars have been the primary sensor for probing clouds and precipitation, serving a wide spectrum of applications ranging from climate studies to severe weather monitoring [*Kollias et al.*, 2019]. For data record continuity reasons among others, the majority of scanning radars have been operated with predetermined scan strategies not always optimum for the specific weather conditions at hand [*McLaughlin et al.*, 2009; *Miller et al.*, 1998].

Besides the handful of weather-chasing mobile scanning radars guided by expert field researchers (e.g., [*Bluestein et al.*, 2010; *Pazmany et al.*, 2013; *Wurman et al.*, 1997]), only a few scanning radars systematically adapt their sampling strategy based on the actual atmospheric state. An example of this is the Collaborative Adaptive Sensing of the Atmosphere (CASA) network [*McLaughlin et al.*, 2009]; a network of small, low-cost, short-range radars controlled by a software architecture, which automatically balances user preferences for information, data quality, system resources, and the evolving weather [*Philips et al.*, 2008]. Other examples include the large mechanically scanning Chilbolton radar, which is steered towards storms automatically based on their size, rainfall rate, and distance from the radar [*Stein et al.*, 2015], as well as the U.S. National Weather Service Weather Surveillance Radar-1988 Doppler (NEXRAD) network, which switches between clear-air and precipitation mode based on the weather [*Chrisman*, 2009].

One common characteristic of current adaptive scan strategies (including the aforementioned) is that they rely on measurements collected by the radar itself while in surveillance mode to sense the atmospheric state and identify targets of interest. We will call this approach "stand-alone", highlighting the fact that it only relies on the use of the radar both to provide context and to collect targeted observations. We would argue that the "stand-alone" approach has three main drawbacks: it may not allow for i) the detection of upwind or elevated features outside of the surveillance coverage, ii) the detection of weakly reflective features because the scan rate required for performing surveillance limits sensitivity iii) fast-evolving processes or short-lived systems because surveillance diverts resources away from sampling features of interest.

Here we propose a new radar sampling paradigm that provides greater awareness of the atmospheric state allowing for the collection of more comprehensive and higher quality observations of atmospheric phenomena through the uses of rapid sequences of targeted scans. In this framework, which we call the Multisensor Agile Adaptive Sampling (MAAS) framework, a collection of observations from external sources each uniquely sensitive to different parts of the atmospheric system are used to steer one or multiple scanning observing systems.

This manuscript describes an implementation of this versatile framework used to steer two fundamentally different yet uniquely complementary radars currently operating from the Stony Brook Radar Observatory (SBRO). Guidance by MAAS allowed radars to observe a shallow cloud over its life cycle and elusive short-term phenomena in deeper clouds including waterspouts and lighting-induced ice crystal orientation.

2. Implementation of the Multisensor Agile Adaptive Sampling (MAAS) framework

In this section, we describe an implementation of the MAAS framework used to automatically steer two collocated radars (Sect. 2.1) radars under both shallow (Sect. 2.2) and deep (Sect. 2.3) cloud conditions. At the moment, user input is required to switch between modes.

2.1. Description of the radars

KASPR is a mechanically scanning 0.3º beamwidth Ka-band polarimetric radar, which is an upgraded version of the scanning Atmospheric radiation measurement Cloud Radars (SACRs) described in [*Kollias et al.*, 2014a; *Kollias et al.*, 2014b] (Fig. 1). KASPR collects standard radar moments: radar reflectivity (Z_{HH}), Doppler velocity and spectral width; as well polarimetric radar observables including: differential reflectivity (Z_{DR}), differential phase (φ_{DP}), co-polar correlation coefficient (ρ_{hv}), linear depolarization ratio, cross-polar correlation coefficient (ρ_{hx}) and specific differential phase (K_{DP}) [*Hubbert and Bringi*, 1995]. In the current study, KASPR was set to operate with pulse compression, a range gate spacing of 25 m, maximum range of 30 km and to scan at a rate of 6 ° s^{-1} yielding a sensitivity of -40 dBZ at 1 km.

SKYLER is a dual-polarization, X-band, low-power, phased-array radar (Fig. 1; [*Kollias et al.*, 2018]) with an antenna beamwidth of 1.98° in azimuth and 2.1° in elevation at boresight. The radar transmits H- and V-polarization pulses (alternate) and provides estimates of standard radar moments as well as of Z_{DR}, φ_{DP}, and ρ_{hv}. Relative to its baseline position, SKYLER is capable of electronically scanning a sector of +/- 45° in azimuth and electronically scanning a sector of 0-30° in elevation. SKYLER baseline position is mechanically controlled though not automatically at the moment; for the current study SKYLER was positioned facing south at 15° elevation. SKYLER was set to operate with, a range gate spacing of 100 m and maximum range of 40 km and to scan at a rate of 30 ° s^{-1} yielding a sensitivity better than 0 dBZ at 1 km.

2.2. Shallow cloud systems – Steering of a mechanically scanning cloud radar

Millimeter-wavelength radars, such as KASPR, with their generally excellent sensitivity tend to be preferred for the study of clouds and light precipitation [*Kollias et al.*, 2016; *Kollias et al.*, 2007]. That being said, their narrow antenna beam width requires operation at a slower scan rate in order to collect a sufficient number of samples to achieve detection of low signal-to-noise ratio echoes [*Doviak and Zrnic*, 1993]. Under these conditions, approximately 10-minutes would be required to cover the hemispherical sky (i.e., a 360° azimuth sector at 10 different elevations at 6º s^{-1}) thus rendering impossible the complete sampling, let alone tracking, of fast evolving clouds such as shallow cumuli. Because of this limitation, among other things, millimeter-wavelength radars have typically been operated following a set of predetermined scan strategies, presumably suitable for the characterization of clouds (if so encountered) (e.g., [*Kollias et al.*, 2014a]). Only on few occasions have these systems been fortuitous enough to collect snapshots of fast evolving

atmospheric systems, notably by using range-height indicator (RHI) type scan strategies [*Borque et al.*, 2014; *Lamer et al.*, 2014].

During shallow cloud conditions, the MAAS framework (Fig. 1) addresses the aforementioned challenges using surveillance provided by the ABI onboard the GOES-16 satellite to guide KASPR.

First, a snapshot from the finest spatial resolution (0.5-1 km^2) visible red band (band 2) of the GOES-16 Advanced Baseline Imager (ABI) is used to locate the brightest region within a 50-km radius around the observatory; the latitude and longitude of this feature are converted to azimuthal coordinates, which are sent to KASPR for initial positioning.

The advection speed and direction of the feature are then estimated by maximizing correlation with the next consecutive GOES-16 ABI snapshot within a 10-km radius around the feature (guaranteed available within 5-minutes) and converted to an azimuthal trajectory for subsequent KASPR positioning.

The initial azimuthal positioning and trajectory (for subsequent repositioning) are used to guide either of two scan types – an RHI sequence (Sect. 2.1.1) or a slanted path (Sect. 2.1.2) – each providing unique insight into short-lived shallow clouds. Note that because MAAS does not require the steered system to conduct its own surveillance to provide atmospheric context, it allows for a reduced scan rate, thus generating a gain in sensitivity compared to "stand-alone" operation.

2.1.1 Slicing through a shallow cloud system

When elected by the user, MAAS provides the azimuthal guidance required to perform a sequence of RHI scans tracking a cloud entity. The RHI scans are set to cover an elevation sector between, for example, 1° to 9° at a 0.3° spacing (i.e., no gaps in elevation) and as such target shallow clouds forming and advecting from a distance ~ 15-30 km away from the radar. The limited extent of the elevation sector allows for rapid updates, enabling the characterization of cumulus life cycle, an example of which is given in Sect. 3.1.

2.1.2 Staring at a shallow cloud system

When elected by the user, a slanted path scan is initiated. Slanted path scans additionally require information about the elevation of clouds above the horizon. An assumption about the lifting condensation level height is initially used to steer KASPR in the elevation direction. This position is refined using observations collected by a boresight camera installed on KASPR's pedestal, which records sub-second red-green-blue imagery collocated with the radar beam. A first snapshot ("reference" snapshot) from the boresight camera is used to slightly adjust the KASPR's pointing (both in azimuth and elevation) such that the brightest region within the boresight camera frame is centered. Subsequent snapshots from the boresight camera (every 5 s) are used to estimate/adjust advection speed in the elevation direction and adjust the azimuthal advection position and speed estimates initially obtained using GOES-16 visible imagery. Both are accomplished by maximizing the correlation between the current boresight camera snapshots and the reference boresight camera snapshot. Poor correlation between the snapshots is used as an indication that the feature has dissipated or morphed beyond recognition and triggers the end of the tracking sequence.

2.3. Deep cloud systems – Steering of a centimeter-wavelength phased-array radar and a mechanically scanning cloud radar

Although millimeter-wavelength radars may also provide insight into the properties of precipitation, they generally suffer from non-negligible attenuation; for this reason, centimeter wavelength radars tend to be preferred for the study of precipitation and weather monitoring [*Kollias et al.*, 2019].

In the past few years, the adaptation of phased array technology to atmospheric applications has enabled near instantaneous positioning of the radar beam and nearly simultaneous independent monitoring of multiple spatially separated atmospheric features [*Council*, 2008]. At the moment, only a handful of phased-array systems for atmospheric applications are operational, those include the SBRO's SKYLER system (courtesy of Raytheon Company, [*Kollias et al.*, 2018]) and the National Radar Testbed (NWRT; [*Curtis and Torres*, 2011]).

Despite their more rapid scan rate, phased-array radars are not without shortcomings. Since the elevation sector they can electronically scan is limited, they typically cannot locate the highest point of storms which is often spatially correlated with atmospheric vortices (i.e., tornadoes and waterspouts), especially at short ranges. Furthermore, phased-array radars are challenged when it comes to acquiring high quality polarimetric data [*Zhang et al.*, 2019] suggesting that they could benefit from collaborative sensing with a high-quality, parabolic-dish polarimetric radar. Phased-array systems, like all radars, are also unable to directly detect lightning which is one of the leading cause of weather-related deaths in the United States [*Service*, 2018]; yet when properly steered they have shown capable of providing invaluable insight into the factors leading to lightning cessation [*Preston and Fuelberg*, 2015; *Schultz et al.*, 2011]. A multi-sensor approach to radar guidance could greatly increase the likelihood of collecting the type of observations required to improve our understanding of convective storms.

During deep cloud conditions, MAAS automatically determines the azimuthal position of the SKYLER and KASPR RHI's. SKYLER is set to perform three simultaneous RHI scans while KASPR is set to perform a single RHI scan covering a sector between 2-90° along the path of one of SKYLER's RHI. MAAS relies on information from:

i. "stand-alone" surveillance simultaneously performed by SKYLER, taking the form of a Plan Position Indicator (PPI) scan performed at 10° elevation covering SKYLER's full azimuthal range (+/- 45° azimuth sector relative to the position of its manually steerable rotation table). SKYLER's first simultaneous RHI is aimed toward the azimuth of the highest reflectivity region in the surveillance scan between 0-30 km range.
ii. surveillance provided by the GOES-16 ABI; SKYLER's second simultaneous RHI is aimed toward the azimuth of the coldest cloud top within a 50-km radius around the observatory as identified within observations from band 13 of the GOES-16 ABI (i.e., top-of-atmosphere outgoing longwave radiance, 1-2 km^2 resolution).
iii. surveillance provided by the GOES-16's Geostationary Lightning Mapper (GLM) (9.5-km pixel field of view) that can detect momentary changes in an optical scene for lighting detection (e.g., [*Goodman et al.*, 2013]). Both SKYLER's third

simultaneous RHI and KASPR's RHI are aimed toward the azimuth of the most recent lightning (within one minute) or highest strike density (within five minutes), in that order of precedence. After five minutes of lightning inactivity, SKYLER and KASPR fall back to duplicate the RHI guided by the coldest cloud top (providing doubled temporal resolution for SKYLER).

Note that storm motion is currently not estimated in deep mode such that completion of each RHI leads to the search for a new feature of interest. This mode enabled the observations of several waterspouts and of lighting-induced ice crystal orientation events, examples of which are given in Sect. 3.2 and Sect. 3.3 respectively.

3. Radar observations of fast physics enabled by MAAS

The MAAS framework enabled the agile deployment of KASPR and/or SKYLER for the monitoring of generally elusive shorth-lived atmospheric phenomena including: i) a shallow cumulus cloud along its lifecycle (Sect. 3.1), waterspouts (Sect. 3.2) and ice crystal orientation in a lightening producing storm (Sect. 3.3).

3.1. Shallow cumulus cloud life cycle

On August 25, 2019, a number of fair-weather shallow cumulus clouds were observed to form in the vicinity of the observatory. At 21:15:00 UTC, without any intervention from the KASPR radar, MAAS selected a bright target cloud identified in the GOES-16 visible imagery (along the line Fig. 2a). Following the collection of a second GOES-16 visible image (not shown), the advection speed and direction of this cloud was determined. This allowed MAAS to guide KASPR through a series of RHI scans at azimuthal locations adjusted to follow the estimated cloud trajectory. Because MAAS does not utilize any of KASPRs resources for surveillance, it allows for the uninterrupted collection of several vertical cross sections (i.e., RHIs) within the same evolving cloud. During this event which began at 21:18:51 UTC and ended at 21:27:27 UTC, MAAS enabled KASPR to collect a total of 80 RHI scans each within 3-11 seconds apart proving a uniquely high-resolution uninterrupted view of the rapidly evolving shallow cumulus.

Figures 2 b-e show a subset of the RHI scans collected by KASPR during the event (not consecutive; only ranges between 15-23 km away from the radar location are shown which is depicted by the location of the black line on Fig. 2a). The radar reflectivity field can be used to visualize the roughly 2-km deep cumulus cloud(s) that formed just between 15–23 km away from the radar's location. Note the cellular structure of the cloud(s) with two distinct reflectivity maxima (one between 19.5–20 km and one between 18-19 km). Over time, the initially stronger cell is observed to weaken and the cloud top above it collapsing, while the other cell is observed to intensify and the cloud top above it rising. We estimate, based on the time from when the weaker cell was first observed to when it was last detected, that the cell's life cycle was roughly 9 minutes long.

Hopefully, MAAS will facilitate frequent observations of the internal structure of evolving shallow cumuli within their mesoscale context (as captured by the GOES-16 satellite; Fig. 2a) and contribute to fill in some outstanding gaps in our understanding of shallow cloud lifecycle.

3.2. Waterspouts

On September 2, 2019, the public reported several waterspouts on the south shore of Long Island. A rotation signature visible in the surveillance PPI scan collected by the National Weather Services' NEXRAD radar on Long Island (KOKX) suggests that a waterspout did form near Fire Island at 19:52 UTC (magenta dashed circle in Fig. 3b). Minutes before, SKYLER also performed a PPI surveillance and detected not only one but two rotation signatures within the same sector (magenta dashed circles in Fig. 3c). Based on the collection of subsequent SKYLER surveillance scans we estimate that the waterspouts generally travelled east northeastward and lasted between 10 and 15 minutes.

Besides reporting on the location of these waterspouts with clear horizontal rotation signatures and intensity reflectivity features, KASPR and SKYLER guided by MAAS sliced through a developing waterspout near Fire Island (Fig. 3d,e,f; range covering the black line on Fig. 3c). Not evident in the "stand-alone" surveillance, the location of this developing waterspout coincided with that of multiple lighting flashes detected by the GOES-16 GLM which information is used in the MAAS framework to guide the radars (lighting density in 5-min time windows from 19:40 to 20:20 UTC shown in Fig. 3a). Although nearly simultaneous, the measurements collected by each of the radars differed, thus highlighting their unique complementarity and respective limitations (attenuation by rain for KASPR and lack of sensitivity to cloud for SKYLER). KASPR's measurements reveal the impressive depth of cloud supporting this rotating system, the tops of which extended to 12 km (Fig. 3d) while SKYLER's measurements suggest that at its narrowest point, this waterspout had to be at least 2 km wide (Fig. 3f). SKYLER's Doppler velocity measurements within the core of the waterspout reveal peak wind speeds of 25 m s^{-1} and suggest counterclockwise spiral rotation (as evidenced by the tilted Doppler velocity dipole in Fig. 3f).

Under the automatic guidance of the MAAS framework, KASPR was able to monitor the evolution of this waterspout from its generally poorly documented early stage to its mature stage, intersecting it every 40 seconds while SKYLER RHI's toggled between several waterspouts.

3.3. Ice crystal orientation in a lightning producing storm

On August 21st, 2019, the GOES-16 GLM detected several lightning flashes on the South shore of Long Island (not shown). To gather unique insight on the internal structure of lightning producing convective cells, KASPR, which itself cannot detect lightning, was deployed by MAAS to slice through the convective cell located in the region of greatest lighting flash density reported by the GOES-16 GLM (Fig. 4c,d,e range covering the black line on Fig. 4b).

KASPR recorded a bright band around 4 km suggesting that the storm contained both ice aloft and rain below (Fig. 4c). Below the melting layer, KASPR recorded radar reflectivity as high as 40 dBZ within the convective core (note that radar reflectivity measurements beyond the core are attenuated). Above the melting layer, KASPR recorded negative specific differential phase (K_{DP}, <-4 ° km^{-1}; less affected by attenuation) and large cross-polar correlation coefficient (ρ_{hx}, > 0.6). Combined, these suggest the presence of

prolate ice particles vertically oriented through lightning-induced electrification [*Biggerstaff et al.*, 2017; *Ryzhkov et al.*, 2002].

Under the automatic guidance of the MAAS framework, KASPR was able to monitor the evolution of this lightning producing convective cell, intersecting it every 40 seconds for 80 minutes. Hopefully some of the radar signatures it detected can be associated to processes such as lightning cessation and help in the development of predictive schemes. Additional simultaneous RHIs were also collected by SKYLER (not shown) in the direction of the coldest cloud top (i.e., circle in Fig. 4a and 4b) and the highest reflectivity echo in SKYLER's own PPI surveillance (triangle in Fig. 4b).

4. **Summary and future plans**

Generally speaking, MAAS is a framework that relies on a collection of observations from external sources to steer one or more scanning observing systems. MAAS was designed to overcome challenges associated with relying on a single observing system both for locating, tracking and sampling features of interest, especially for the characterization of fast-evolving cloud and precipitation processes and short-lived atmospheric systems.

Here, we present an implementation of MAAS suitable for the steering of two unique radars: KASPR a mechanically scanning Ka-band polarimetric radar and SKYLER a phased-array X-band polarimetric radar. In this implementation, depending on the atmospheric conditions (shallow or deep clouds), a combination of observations collected by the GOES-16 ABI, the GOES-16 GLM and/or a visible camera installed on KASPR's boresight is used to locate and estimate the advective trajectory of atmospheric feature of interest for their tracking by the radars.

To our knowledge, this constitutes the first time that a high-quality, mechanically scanning polarimetric cloud radar has performed coordinated scans in conjunction with an electronically scanning radar. The mechanically scanning KASPR was dedicated to slow scan rate, high quality vertical cross-section scans while the agile phased-array SKYLER utilized its advantage in near instantaneously interrogating many different parts of a storm and providing high temporal resolution updates. This particular combination of radar resources steered by the MAAS framework has the potential to provide a leap forward in our ability to understand rapidly evolving microphysical and dynamical processes in cloud and precipitation systems.

KASPR and SKYLER guided by MAAS were shown capable of collecting unique information about the internal structure of i) a multi-cell cumulus cloud along its 9-minute life cycle at sub-minute temporal resolution, ii) a forming waterspout and iii) a lightning producing convective system including high-quality polarimetric information suggesting the presence of vertically oriented ice crystals.

In future expansions, MAAS could rely on observations from other operational sensors such as i) the NEXRAD which provides information about far range targets, ii) networks of surface cameras and iii) lidars sensible to cloud base height and clear air dynamics. As a fail-safe, MAAS could also be expanded to be completely "stand-alone". This possibility is already implemented in the "deep cloud mode" and could easily be implemented in the "shallow cloud mode" by for example having KASPR perform 1 PPI scan at an arbitrary elevation and then having it scan through the highest reflectivity target identified in that surveillance scan. The MAAS framework could also be used to manage

sensor operations in power limited environments like buoys and CubeSat's [*Peral et al.*, 2019].

5. Acknowledgements

Special thanks to Raytheon Company. The authors are supported by the Department of Energy Atmospheric System Research program. All the data used can be found in the Stony Brook University repository at https://commons.library.stonybrook.edu/somasdata/.

7. References

Biggerstaff, M. I., Z. Zounes, A. A. Alford, G. D. Carrie, J. T. Pilkey, M. A. Uman, and D. M. Jordan (2017), Flash propagation and inferred charge structure relative to radar-observed ice alignment signatures in a small Florida mesoscale convective system, *Geophysical Research Letters*, *44*(15), 8027-8036.

Bluestein, H. B., M. M. French, I. PopStefanija, R. T. Bluth, and J. B. Knorr (2010), A Mobile, Phased-Array Doppler Radar For The Study of Severe Convective Storms, *Bulletin of the American Meteorological Society*, *91*(5), 579-600, doi:10.1175/2009bams2914.1.

Borque, P., P. Kollias, and S. Giangrande (2014), First observations of tracking clouds using scanning ARM cloud radars, *Journal of Applied Meteorology Climatology*, *53*(12), 2732-2746.

Chrisman, J. N. (2009), Automated volume scan evaluation and termination (AVSET), paper presented at 34th Conference on Radar Meteorology.

Council, N. R. (2008), *Evaluation of the multifunction phased array radar planning process*, National Academies Press.

Curtis, C. D., and S. M. Torres (2011), Adaptive range oversampling to achieve faster scanning on the National Weather Radar Testbed Phased-Array Radar, *Journal of Atmospheric and Oceanic Technology*, *28*(12), 1581-1597.

Doviak, R., and D. Zrnic (1993), Doppler radar and weather observations academic, *San Diego, Calif*.

Goodman, S. J., R. J. Blakeslee, W. J. Koshak, D. Mach, J. Bailey, D. Buechler, L. Carey, C. Schultz, M. Bateman, and E. McCaul Jr (2013), The GOES-R geostationary lightning mapper (GLM), *Atmospheric research*, *125*, 34-49.

Hubbert, J., and V. Bringi (1995), An iterative filtering technique for the analysis of copolar differential phase and dual-frequency radar measurements, *Journal of Atmospheric and Oceanic Technology*, *12*(3), 643-648.

Kollias, P., N. Bharadwaj, E. Clothiaux, K. Lamer, M. Oue, J. Hardin, B. Isom, I. Lindenmaier, A. Matthews, and E. Luke (2019), The ARM Radar Network: At the Leading-edge of Cloud and Precipitation Observations, *Bulletin of the American Meteorological Society*(2019).

Kollias, P., N. Bharadwaj, K. Widener, I. Jo, and K. Johnson (2014a), Scanning ARM cloud radars. Part I: Operational sampling strategies, *Journal of Atmospheric and Oceanic Technology*, *31*(3), 569-582.

Kollias, P., E. E. Clothiaux, T. P. Ackerman, B. A. Albrecht, K. B. Widener, K. P. Moran, E. P. Luke, K. L. Johnson, N. Bharadwaj, and J. B. Mead (2016),

Development and applications of ARM millimeter-wavelength cloud radars, *Meteorological Monographs*, *57*, 17.11-17.19.

Kollias, P., I. Jo, P. Borque, A. Tatarevic, K. Lamer, N. Bharadwaj, K. Widener, K. Johnson, and E. E. Clothiaux (2014b), Scanning ARM cloud radars. Part II: Data quality control and processing, *Journal of Atmospheric Oceanic Technology*, *31*(3), 583-598.

Kollias, P., D. McLaughlin, S. Frasier, M. Oue, E. Luke, and A. Sneddon (2018), Advances and applications in low-power phased array X-band weather radars, paper presented at 2018 IEEE Radar Conference (RadarConf18), IEEE.

Kollias, P., M. A. Miller, E. P. Luke, K. L. Johnson, E. E. Clothiaux, K. P. Moran, K. B. Widener, and B. A. Albrecht (2007), The Atmospheric Radiation Measurement Program cloud profiling radars: Second-generation sampling strategies, processing, and cloud data products, *Journal of Atmospheric and Oceanic Technology*, *24*(7), 1199-1214.

Lamer, K., A. Tatarevic, I. Jo, and P. Kollias (2014), Evaluation of gridded scanning ARM cloud radar reflectivity observations and vertical doppler velocity retrievals, *Atmospheric Measurement Techniques*, *7*(4), 1089-1103.

McLaughlin, D., D. Pepyne, V. Chandrasekar, B. Philips, J. Kurose, M. Zink, K. Droegemeier, S. Cruz-Pol, F. Junyent, and J. Brotzge (2009), Short-wavelength technology and the potential for distributed networks of small radar systems, *Bulletin of the American Meteorological Society*, *90*(12), 1797-1818.

Miller, M. A., J. Verlinde, C. V. Gilbert, G. J. Lehenbauer, J. S. Tongue, and E. E. Clothiaux (1998), Detection of nonprecipitating clouds with the WSR-88D: A theoretical and experimental survey of capabilities and limitations, *Weather and forecasting*, *13*(4), 1046-1062.

Pazmany, A. L., J. B. Mead, H. B. Bluestein, J. C. Snyder, and J. B. Houser (2013), A mobile rapid-scanning X-band polarimetric (RaXPol) Doppler radar system, *Journal of Atmospheric and Oceanic Technology*, *30*(7), 1398-1413.

Peral, E., S. Tanelli, S. Statham, S. Joshi, T. Imken, D. Price, J. Sauder, N. Chahat, and A. Williams (2019), RainCube: the first ever radar measurements from a CubeSat in space, *Journal of Applied Remote Sensing*, *13*(3), 032504.

Philips, B., D. Westbrook, D. Pepyne, J. Brotzge, E. J. Bass, and D. Rude (2008), User evaluations of adaptive scanning patterns in the CASA spring experiment 2007, paper presented at IGARSS 2008-2008 IEEE International Geoscience and Remote Sensing Symposium, IEEE.

Preston, A. D., and H. E. Fuelberg (2015), Improving lightning cessation guidance using polarimetric radar data, *Weather and Forecasting*, *30*(2), 308-328.

Ryzhkov, A. V., D. S. Zrnic, J. C. Hubbert, V. Bringi, J. Vivekanandan, and E. A. Brandes (2002), Polarimetric radar observations and interpretation of co-cross-polarcorrelation coefficients, *Journal of Atmospheric and Oceanic Technology*, *19*(3), 340-354.

Schultz, E. V., W. A. Petersen, and L. D. Carey (2011), Exploring the use of radar for a physically based lightning cessation nowcasting tool.

Service, N. W. (accessed on 2018) Weather Related Fatality and Injury Statistics, https://www.weather.gov/hazstat/

Stein, T. H., R. J. Hogan, P. A. Clark, C. E. Halliwell, K. E. Hanley, H. W. Lean, J. C. Nicol, and R. S. Plant (2015), The DYMECS project: A statistical approach for the evaluation of convective storms in high-resolution NWP models, *Bulletin of the American Meteorological Society*, *96*(6), 939-951.

Wurman, J., J. Straka, E. Rasmussen, M. Randall, and A. Zahrai (1997), Design and deployment of a portable, pencil-beam, pulsed, 3-cm Doppler radar, *Journal of Atmospheric and Oceanic Technology*, *14*(6), 1502-1512.

Zhang, G., V. N. Mahale, B. J. Putnam, Y. Qi, Q. Cao, A. D. Byrd, P. Bukovcic, D. S. Zrnic, J. Gao, and M. Xue (2019), Current status and future challenges of weather radar polarimetry: Bridging the gap between radar meteorology/hydrology/engineering and numerical weather prediction, *Advances in Atmospheric Sciences*, *36*(6), 571-588.

Figures

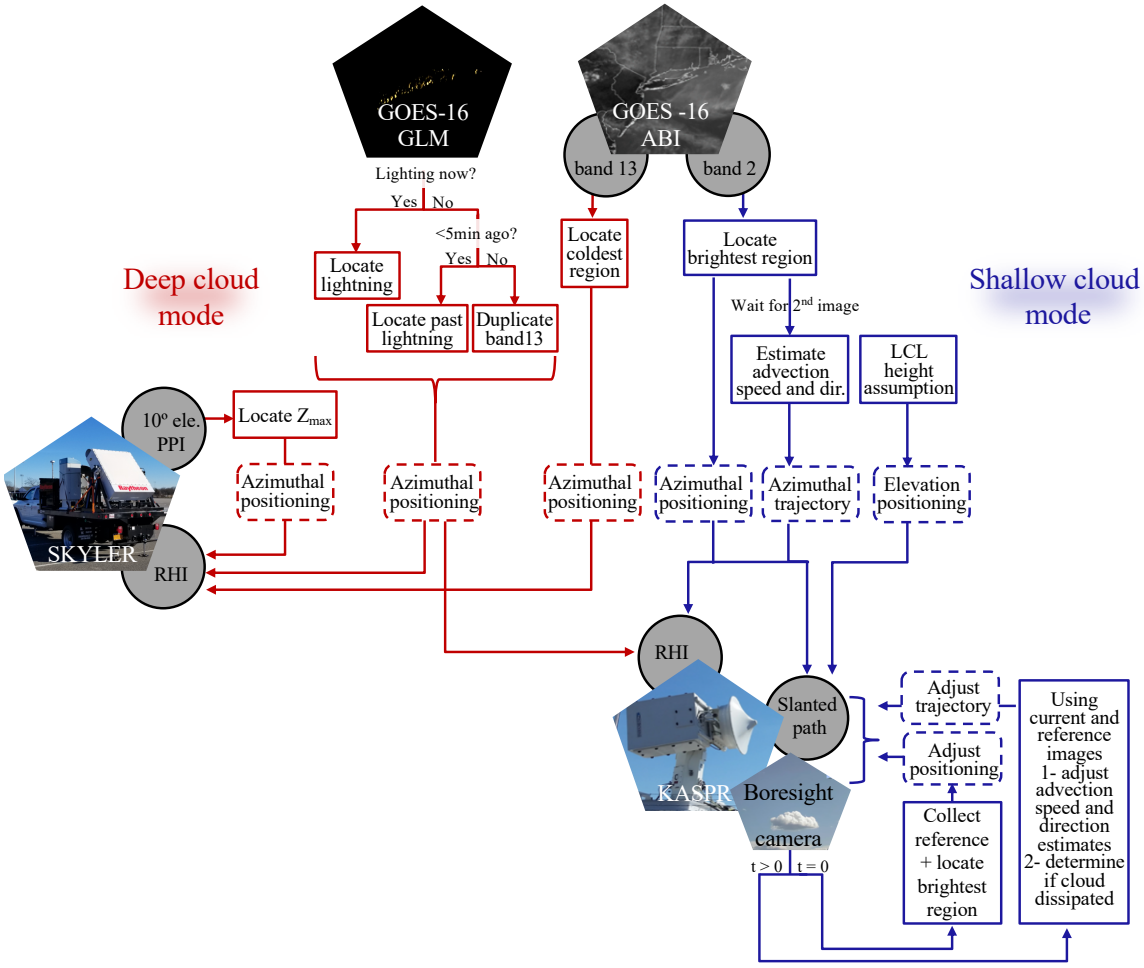

Figure 1. The MAAS framework is used to guide the scan strategy of the KASPR and the SKYLER radars using inputs from multiple sensors.

.

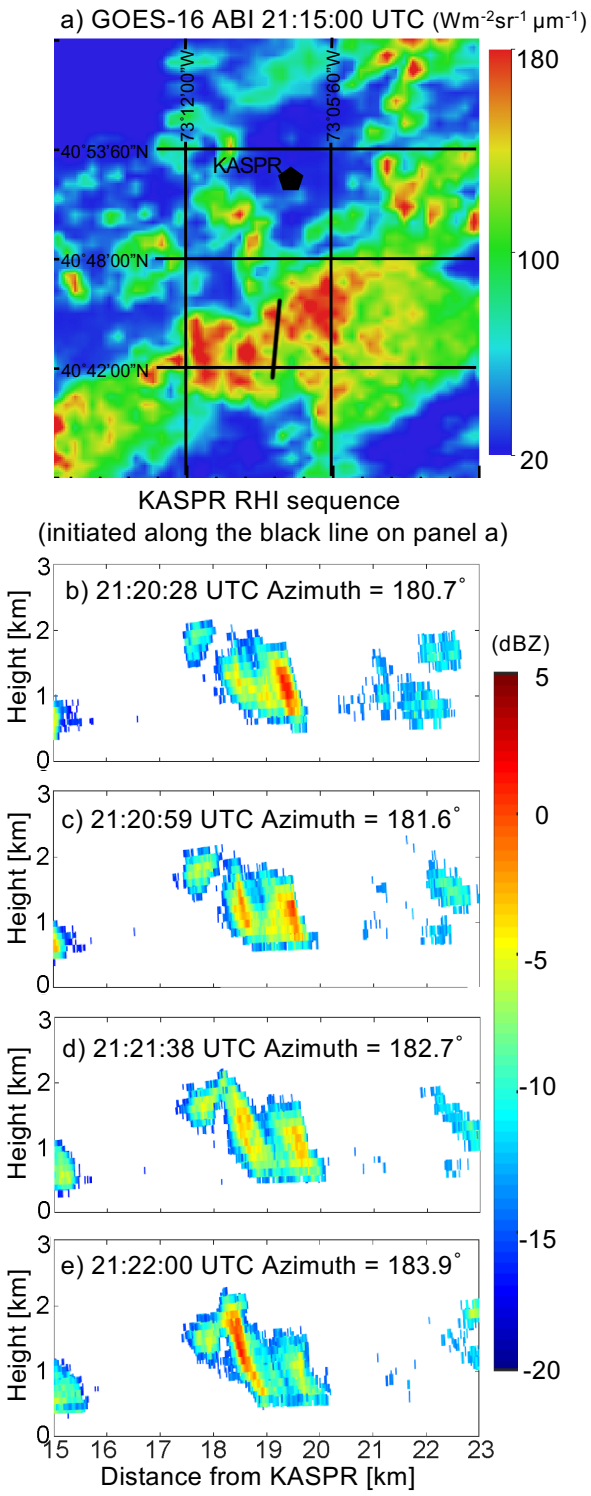

Figure 2. a) Radiance recorded by GOES-16 ABI, b-e) radar reflectivity recorded by the KASPR during an RHI sequence guided by the MAAS framework; The RHI scan sequence was initiated along the line depicted in panel (a) and the azimuthal position updated following MAAS guidance.

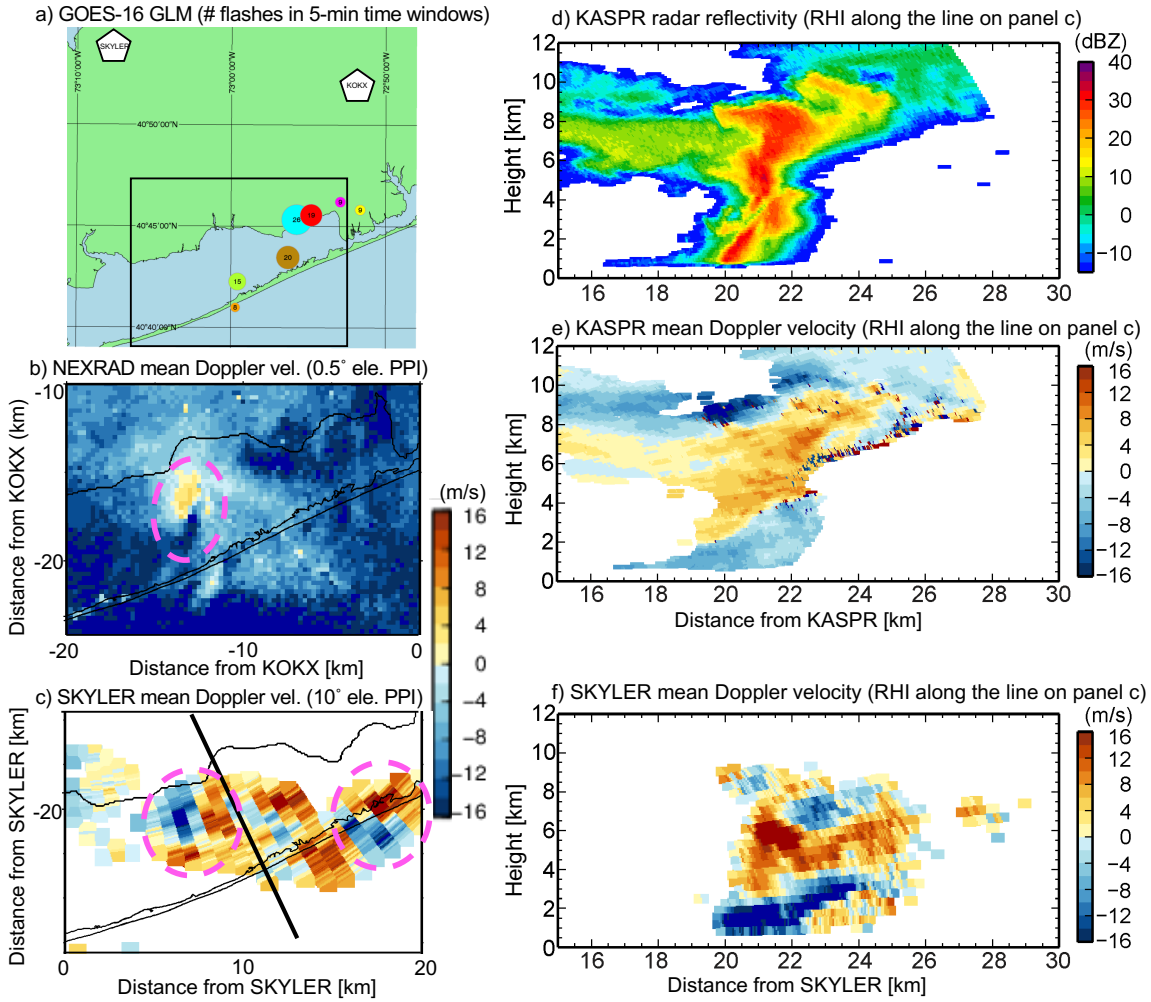

Figure 3. a) Lighting strike density in 5-min time windows from 19:40 to 20:20 UTC (orange, green, brown, turquoise, red and magenta respectively) estimated from the GOES-16 GLM. For the region within the black rectangle in panel (a), b) Doppler velocity recorded by the NEXRAD radar during a PPI scan at 19:52 UTC. c) Doppler velocity recorded by the SKYLER during a PPI scan at 19:45 UTC. Magenta dashed circles indicate rotation signatures in panels (b) and (c). d-e) radar reflectivity and Doppler velocity recorded by the KASPR during an RHI scan directed towards a lightning strike observed by the GOES-16 GLM along the trajectory marked by the black line on panel (c). f) Doppler velocity simultaneously recorded by SKYLER for the same location. Note that negative Doppler velocity indicate motion towards the radars.

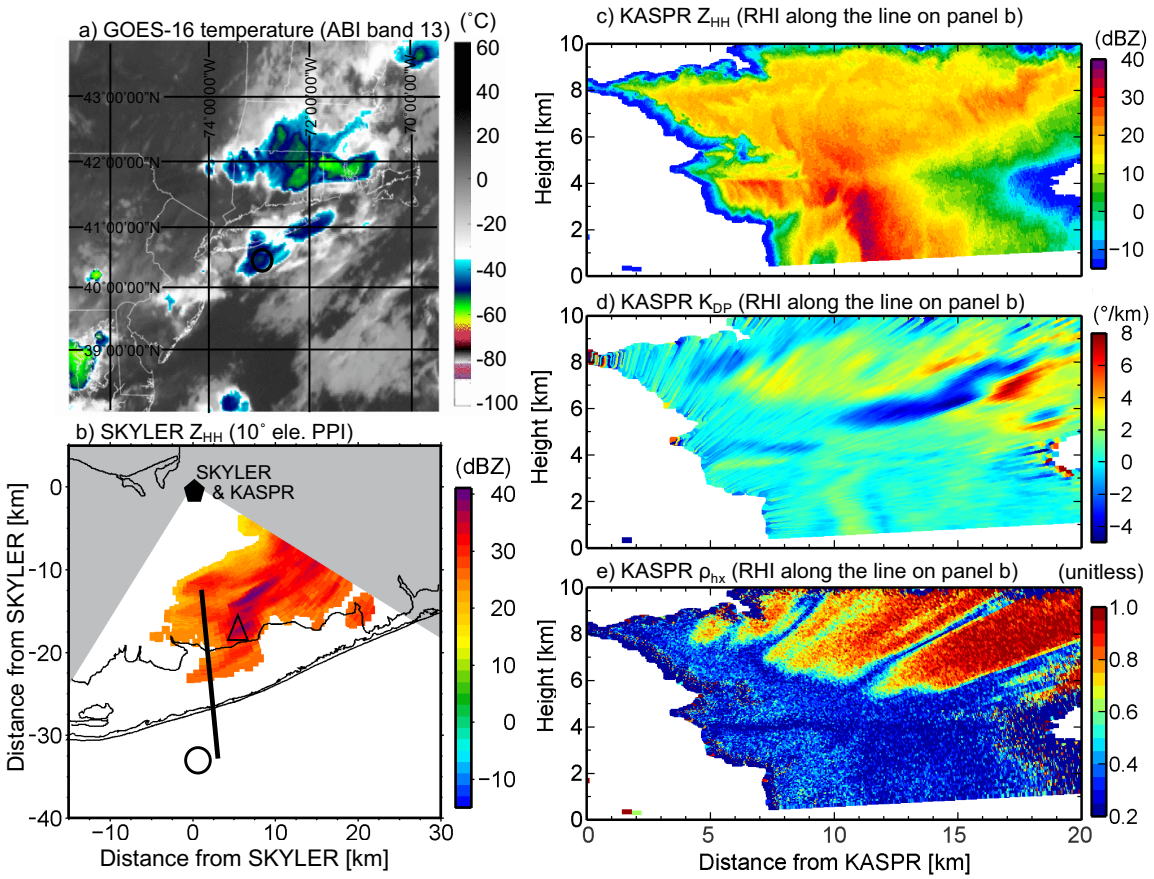

Figure 4. a) Cloud top temperature recorded by the GOES-16 ABI at 23:27 UTC, b) radar reflectivity recorded by SKYLER during a PPI scan at 23:30 UTC. c) Radar reflectivity, d) K_{DP}, and e) ρ_{hx} recorded by KASPR during an RHI scan directed towards a lightning strike observed by the GOES-16 GLM along the trajectory marked by the black line on panel (b). Under guidance from MAAS, RHIs were also collected by SKYLER in the direction of the coldest cloud top [circle in panel (a) and (b)] and the highest reflectivity echo in SKYLER's PPI surveillance [triangle in panel (b)].